

Dark region observed in fluorescence under the condition of a quadrupole magnetic field

Quan Long,* Shuyu Zhou, Shanyu Zhou, and Yuzhu Wang

Laboratory for Quantum Optics, Shanghai Institute of Optics and Fine Mechanics of Chinese Academy of Sciences, P.O. Box 800211, Shanghai 201800, China

(Received 10 January 2000; revised manuscript received 11 April 2000; published 18 July 2000)

We report an experimental observation of a dark region, around the zero-field point of a spheric quadrupole magnetostatic field, in spatial fluorescence emitted by dilute vapor atoms, which were excited by a circularly polarized traveling-wave laser tuned to a $F \rightarrow F+1$ transition of ^{87}Rb . By ruling out some possible sources, we show that the fluorescence decrease is associated with the three-dimensional nature of the magnetic field; it is a consequence of a precession of magnetic dipole moments induced by the radial magnetic field, which significantly cancels the orientation caused by optical pumping near the point of level crossing in the presence of the axial magnetic field. In an alternative way, the phenomenon can be understood as resulting from a destructive quantum interference, which is related to a coherent double-quantum coupling of atomic levels with two fields; one is the laser field, the other is the magnetic field. Analytic expressions for the half-width and contrast of the dark region have been obtained with a simplified model in the limit of low laser power. A qualitative agreement between the theory and experiment is found. The relevance of our study to laser cooling and trapping in a widely used magneto-optical trap based on such a quadrupole magnetic field is discussed. Finally, some applications of the phenomenon are also presented.

PACS number(s): 32.80.Bx, 32.50.+d, 32.60.+i, 32.80.Qk

I. INTRODUCTION

In the past few decades, the process of modifying the standard radiation properties of an atom has attracted much attention (where by “standard” we mean the resonance fluorescence emitted in free space by a two-level system driven by a single near-resonant electromagnetic field.) Some researchers revealed that spontaneous emission can be reduced or enhanced by changing the environment into which an excited atom decays, such as putting the atom into a resonator whose radiation mode density is made different from that of free space [1], or immersing the atom in a squeezed vacuum where some of the radiation modes are squeezed [2]. In some studies, the influence of statistical properties of the driving field on the resonance fluorescence was considered. Related models include those illuminating the atom with a light of different fluctuation characteristics or a nonclassical state in addition to the coherent one usually used [3]. Some investigations paid attention to the interatomic cooperation, which is attributed to the reabsorption of the emitted resonance fluorescence photons by another atom in a many-atom system. Such an effect, known as radiation trapping, can effectively change the average lifetime of the ensemble of excited atoms [4] and plays an important role in fluorescence when the atomic density is high enough, e.g., when atoms are trapped in a small volume [5]. Other theoretical proposals and experimental works were devoted to achieving a modification of the spontaneous emission rate by taking advantage of the atom’s internal multilevel structure and the effect of quantum interference between multiple atomic transition pathways [6–23]. In these treatments, in addition to the usual driving field, another field is applied to couple some of the atomic levels and establish a coherence between them. The

second field can be a laser light [8,10–13,15,17–23], a microwave or Raman process via an auxiliary level [14,16], or simply the vacuum field [6,7,9]. Compared with methods using a cavity or a squeezed light, the method of quantum interference which requires only free space appears to be easier to realize, and has received great interest recently, especially related to its applications to aspects such as the laser cooling and quantum optics [24,25].

Destructive quantum interference, including scattering-path interference (SPI) [6–11] and the coherent-population trap (CPT) [12–24], may lead to a suppression or partial reduction of fluorescence. SPI refers to the interference between different spontaneous Raman-scattering paths, or the scattering probability amplitudes for routes from a single ground state coherently excited by a monochromatic field to two (or more) intermediate states, from where they spontaneously decay to a final ground state. The interference depends on the coupling between two upper states and the scalar product of the electric dipole moments for transitions sharing the common final state. If the dipole moments are parallel, a destructive SPI may cause a quenching in “total” fluorescence under certain conditions (where by “total” we mean either a spontaneous emission spectrum or fluorescence in all emitted and all polarized directions). If the dipole moments are not parallel, however, there may be only some reduction of fluorescence in certain radiation directions or polarizations, such as the case of the classical Hanle effect, where the dipole moments for σ^+ and σ^- transitions are orthogonal [26]. In the latter case, the decrease in certain directions may be compensated for by an increase in other directions, and results in no modification in total fluorescence. The simplest CPT may occur in the presence of two fields coupling two lower (upper) states with one upper (lower) state and constituting a three-level Λ -(V -) type system, where atoms can be trapped in a coherent superposition of two lower states for the Λ -type system or two laser-dressed states both contaminated by the common lower state for the V -type system. These level structures are typical ones

*Email address: longq4@sina.com

used in double-resonance experiments [27]. At the resonance condition for the double quantum transition, sometimes called the maximum two-photon coherence, the total fluorescence reaches a minimum. More complicated CPT structure involves multiple-quantum-well transitions [22,24].

Recently, Renzoni *et al.* [22] carried out a careful study of the CPT phenomenon on a sodium atomic beam by means of a Hanle effect configuration. In their experiment, atoms were excited by a monochromatic linearly polarized laser light resonant with a hyperfine optical transition $F_g \rightarrow F_e \leq F_g$; the degeneracy of the Zeeman sublevels was removed by applying a dipole magnetic field coaxial with the laser light, and the fluorescence emitted by the atoms at the right angles with respect to the direction of the laser propagation was detected through a photomultiplier. The magnetic field was created by a pair of Helmholtz coils. By scanning the magnetic field, a sharp decrease of the fluorescence intensity (i.e., black line or dark resonance) can be observed at the zero value of the magnetic field, where the resonance condition for a stimulated Raman transition formed by σ^+ and σ^- lights can be achieved. The dependence of the black line, characterized by its half-width and contrast, on the atom-laser interaction parameters, such as the laser intensity, has been examined.

In this paper, we report an experimental observation of a dark region, around the zero-field point of a spheric quadrupole magnetostatic field, in spatial distribution of the fluorescence emitted by dilute atom vapor when excited by a circularly polarized unidirectional propagating laser beam, which was tuned to near the resonance of a $J_g \rightarrow J_e = J_g + 1$, $F_g \rightarrow F_e = F_g + 1$ transition [28]. Modifications of fluorescence were also recorded for other laser configurations, e.g., circularly polarized standing-wave and linearly polarized cases. In our experiment, the magnetic field was produced by a pair of anti-Helmholtz coils (with opposing currents). Several differences between our experiment and that in Ref. [22]. First, the optical transition we used is irrelevant to the CPT discussed by Renzoni *et al.*, because it does not contain a similar coherent superposition noncoupled to the laser, and therefore the mechanisms for fluorescence decrease should be different. Second, the magnetic field presented in our experiment is a quadrupole one of three dimensionality, although the dipole magnetic field in Ref. [22], when its amplitude and direction were varied, can be treated as a one-dimensional (1D) quadrupole field.

An investigation shows that the 3D nature of the magnetic field is the key to understanding what we have observed, especially for the case of a circularly polarized laser, which is the subject that we will focus our attention on in this paper. It is found that, different from the magnetic field in Ref. [22], which was not an origin of the fluorescence decrease and which was utilized merely to tune the Raman transition formed by lights, the magnetic field in our experiment directly takes part in constructing a configuration leading to a fluorescence decrease; the laser light alone cannot account for the modification of the fluorescence. In this configuration, the magnetic field, or more precisely, the radial magnetic field perpendicular to the laser beam, would play the role of a second field like that in Refs. [6–23]. The in-

teraction of the atom with both the laser and the magnetic field leads to a destructive quantum interference effect, i.e., atoms may be trapped in some dressed states mainly composed of metastable states, and exhibits a dark in fluorescence.

The quadrupole magnetic field is well known for its application in atom cooling and trapping. With the aid of three pairs of $\sigma^+ - \sigma^-$ lasers, it constructs a magneto-optical trap (MOT). Some researchers also noted some dark regions along the laser beams when working on MOT's [29]. In contrast to what we report, these regions would not remain still at a fixed place, i.e., the central part of the trap, but would instead move along the beam when tuning the laser frequency. We show, in Sec. IV C, that the phenomenon they observed actually has a very different origin from that presented in this paper. It can be interpreted as a result of saturation hole burning by considering a 1D magnetic field parallel to the laser beam. In fact, two types of dark regions can exist simultaneously in a 1D $\sigma^+ - \sigma^-$ scheme, but if 3D $\sigma^+ - \sigma^-$ lights are introduced as in a MOT, the one fixed around the zero-field point will simply disappear, and leave only the other one, which can be shifted out of the light intersecting region, visible.

Our observation points out the importance of the role played by the radial magnetic field when considering the interaction of an atom with both light and a 3D magnetic field. This fact may require us to reassess the current theory about the cooling and trapping process in MOT's, where the function of the radial magnetic field is always neglected. In Sec. V, we argue that the involvement of the radial magnetic field may affect the polarization gradient cooling in MOT's. Another consequence of the phenomenon is related to the choice of repump laser in MOT's. If a repump laser is chosen to be circularly polarized and tuned to a resonant $\Delta F = F_e - F_g = 1$ transition, our research shows that some atoms, near the trap center, may be confined in the lower hyperfine level of the ground state due to the presence of the radial magnetic field, and cannot be pumped to the higher hyperfine level. Therefore, the power, polarization status, and propagation of the repump laser may not be arbitrary if one wants to gain a favorable repumping efficiency.

The effect of the sharp decrease in fluorescence in the central region may be helpful in the alignment of three orthogonal laser beams in MOT's to make the center of their intersecting region overlap the magnetic field zero; this is important in the process of transferring a MOT to an optical molasses. The phenomenon can also be utilized, in combination with the saturation burning hole, to measure the real magnetic field in MOT's [30].

This paper is arranged as follows. Our experimental setup is given in Sec. II. In Sec. III, the experimental results and a theoretical analysis are presented. Based on an optical Bloch equation, with a simplified model in the limit of low laser power, analytical expressions for the fluorescence intensities with variables of clear physical meanings are obtained for the case of a circularly polarized traveling wave. We argue in Sec. IV that the phenomenon observed can be interpreted in terms of a quantum interference effect. In this section, we also discuss some possible causes of fluorescence decrease,

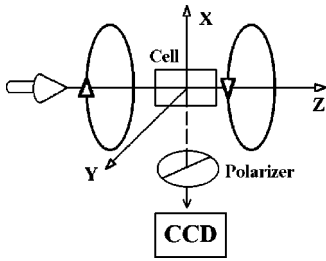


FIG. 1. The experimental setup.

as well as fluorescence modification in other cases with different laser configurations. In Sec. V, we draw our conclusions. The significance and applications of the phenomenon are also described in detail in this last section.

II. EXPERIMENTAL SETUP

Here we describe some principal apparatus used in our experiment. Some others, whenever necessary, will be mentioned in the following sections. The experiment setup is shown in Fig. 1. A six-window uncoated vacuum chamber (actually a vertical cylinder, which has been simplified in the plot), 10 cm in diameter, was filled with a nature rubidium atom vapor with a pressure of 10^{-7} – 10^{-6} Pa at room temperature 300 K. A pair of anti-Helmholtz coils with opposing currents, which generated the spheric quadrupole magnetic field, was mounted on two chamber windows. We used a single-mode Coherent model 899 Ti:sapphire laser actively locked to a crossover resonance of a ^{87}Rb D_2 line in a saturated absorption cell, associated with a computer-controlled servo system; this enabled us to determine the laser frequency with an accuracy of ~ 1 MHz. The laser was a circularly polarized traveling wave tuned near the D_2 line's L_3 peak of ^{87}Rb , $5^2S_{1/2}, F=2 \rightarrow 5^2P_{3/2}, F=3$, and was collimated to pass through the vacuum chamber along the symmetry axis of the coils (defined as the z axis). The laser power measured in the experiment had an uncertainty of $\sim 5\%$ due to the intrinsic fluctuations in light and the systematic error in the power meter. The fluorescence emitted by atoms in a direction (x axis) at a right angle to the incident laser beam was collected and imaged by a charge-coupled device (CCD) camera (Photometrics CH350/L). This camera has a CCD chip, cooled to about -40°C by a thermoelectric cooler, with 1024×1024 pixels of $24 \times 24\text{-}\mu\text{m}^2$ size. The resolution of the image, under the conditions of experiment, was ~ 0.02 cm. In addition, we have used a polarizer, placed in front of the lens of the CCD, to detect the polarization of the fluorescence.

III. EXPERIMENTAL RESULTS AND ANALYSIS

From the camera pictures of the unpolarized fluorescence (with all polarizations taken into account), we observed, around the zero-field point, that there existed a barlike dark region across the beam, illustrating a decrease of fluorescence. This is shown, in Fig. 2(a), as a dip in the profile of the fluorescence intensity versus the space. The zero-field point is theoretically the geometric center of the cell. In fact,

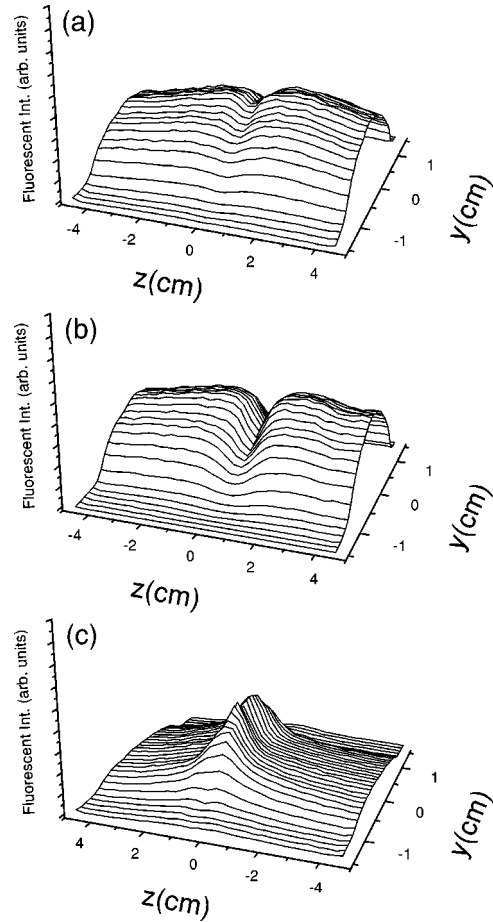


FIG. 2. Spatial fluorescence distribution with a laser intensity 18 mw cm^{-2} , a diameter of the laser beam of 2 cm, a coil current 2.5 A ($\sim 18\text{ G/cm}$ magnetic-field gradient), and a detuning -10 MHz. (a) Unpolarized, (b) y -polarized, and (c) z -polarized fluorescences.

due to residual external magnetic fields (including that of the earth) and some asymmetry between the intensities of two coil currents, it may deviate from the center. The position of the dip could be ensured by another way: Applying three pairs of orthogonal $\sigma^+ - \sigma^-$ standing waves with a repump laser, we could trap a ball-shaped cold atom cloud, and it was not hard to find that the center of the trap (the brightest portion of the cloud) lay in the place of the dark region. Furthermore, if shutting off either pair of beams in x - y plane to form a 2D MOT, we could also observe that the slim cigar-shaped MOT overlapped the dark region. As we know that, for well-aligned MOT beams with excellent balance between partners of each pair of beams, the center of the cloud is always at the field zero [31,32], the above facts demonstrate that the dip is indeed around the zero-field point.

When we applied a polarizer in front of the CCD, it was interesting to note that the central region became darker or turned to be bright for y - or z -polarized fluorescence, shown in Figs. 2(b) and 2(c), respectively. The polarizer used here may help us to distinguish the central dark region from another dark region which may be moved when the laser frequency scanning (see Sec. IV C). A comparison between

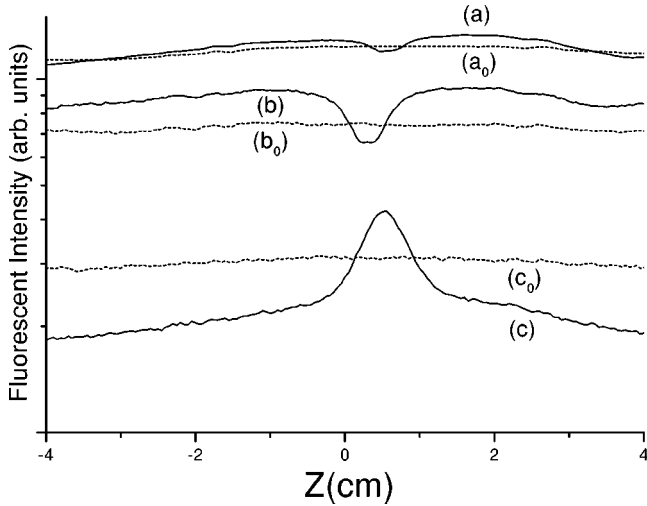


FIG. 3. Comparison of the fluorescence intensity distributions along the z axis for $y \approx 0$ cm between cases with and without a quadrupole magnetic field. The solid lines are for the same parameters as in Fig. 2. The dashed lines (a_0), (b_0), and (c_0) are the corresponding curves when the field is switched off.

cases with and without quadrupole magnetic field is given in Fig. 3. The dip can be characterized by two parameters, half-width [the full width between half minimums, i.e., $(I_{\max} + I_{\min})/2$, with I_{\min} and I_{\max} corresponding to the minimum and maximum values of the dip] and contrast [defined as $(I_{\max} - I_{\min})/(I_{\max} + I_{\min})$], which are about 0.1–1 cm and 1%–5%, respectively, for various magnetic-field gradients and laser powers. We have investigated in detail the influence of laser power, magnetic-field gradient (proportional to the current in the coil), and detuning on the dip in unpolarized fluorescence. A summary of the results is presented in Figs. 4–6: (i) Enhancing the laser power will lead to a wider dip with a larger contrast, [33] which begins to vary slowly for a large laser intensity (Fig. 4). (ii) With an increasing magnetic-field gradient, the dip tends to be narrower and deeper. For a large enough gradient, the contrast exhibits a saturation (Fig. 5). (iii) The location of the dip is insensitive to the detuning, which may otherwise introduce an asymmetry in the profile (Fig. 6). The diameter of the laser beam is not very important (we have also used sheetlike laser beams in the experiment, and obtained similar results), but if it is too thin (approximately < 0.5 cm under our experimental condition when the beam was collinear with the z axis), it will be hard to observe the dark region. Moreover, in order to gain a high signal-to-noise ratio, neither the vapor pressure nor the laser power should be too low.

If the laser frequency is tuned to another $\Delta F = 1$, i.e., the $F_g = 1 \rightarrow F_e = 2$ transition, the result is nearly the same. In addition, similar central dark regions have also been found in the configurations of 1D $\sigma^+ - \sigma^+$ and 1D $\sigma^+ - \sigma^-$ standing waves, except that the contrasts of the dip were somewhat smaller than that of the 1D σ^+ traveling wave. We have also studied a situation in which the laser was linearly polarized. It was found that, for unpolarized fluorescence, the modification of its intensity at the central region depends on the

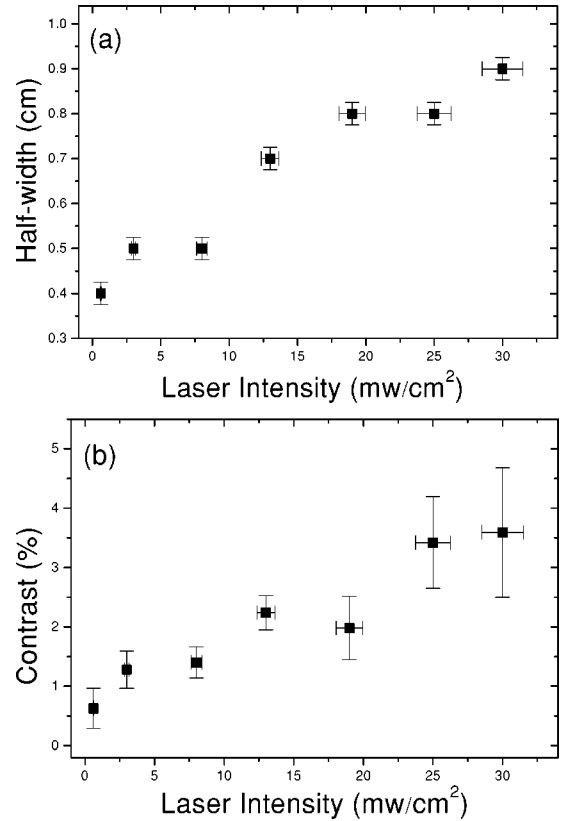


FIG. 4. The variation of (a) the half-width and (b) the contrast of the dip in unpolarized fluorescence vs the laser power for $y \approx 0$ cm. The experimental parameters are coil current 2.5 A, beam diameter 1.5 cm, and near resonance.

plane of light polarization: For a π_x (with an electric field oscillating parallel to the x axis) laser, it was a dip; for a π_y laser, it was a peak [34].

In this section, we will focus on analyzing the configuration of 1D σ^+ traveling wave, because some disturbing facts can be excluded in this case (see Secs. IV C–IV E). At first sight, one may wonder whether the phenomenon is simply a result of the splitting of degenerate Zeeman sublevels in the presence of the z -directional magnetic field. We can easily show that the longitudinal magnetic field B_z alone cannot account for the dip in the fluorescence at $z=0$ for a circularly polarized laser; however, for a linearly polarized laser, taking account of this one-dimensional magnetic field is enough. When the laser is circularly polarized with respect to the quantization axis along the z direction, a ground state can only be optically excited to a pure state, and the atom transition can be treated as a two-level one. Therefore, the level splitting will not cause a special at the point of level crossing, i.e., $z=0$. However, for a linearly polarized case, the situation will be different, as the laser is mixed polarized with σ^+ and σ^- . Instead of a more rigorous quantum-mechanical treatment, the effect of B_z can be estimated by applying a classical model where an excited atom is represented by a single damped oscillating electron. The fluorescence observed in the x direction takes a form, in the far zone,

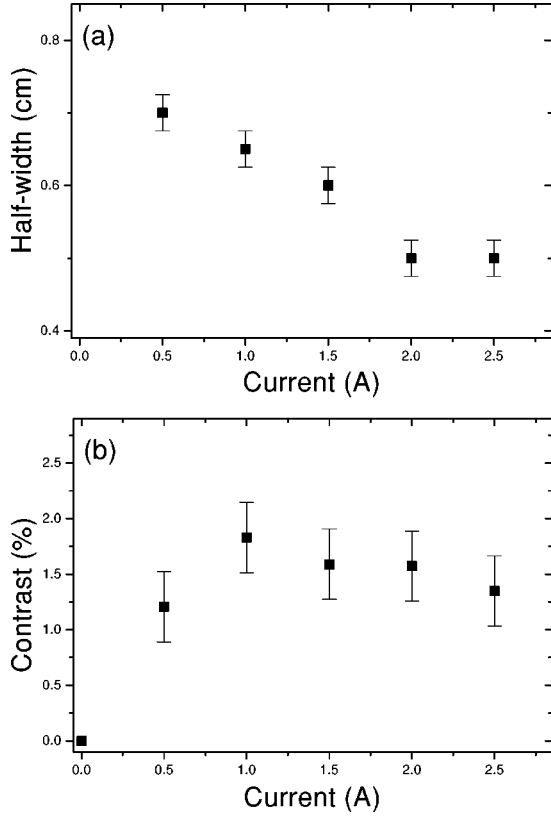


FIG. 5. The variation of (a) the half-width and (b) the contrast of the dip in unpolarized fluorescence vs the magnetic gradient (represented by the coil current) for $y \approx 0$ cm. The experimental parameters are laser intensity 3 mW cm^{-2} , beam diameter 1.5 cm, and near resonance.

$$I_x(\mathbf{r}, t) = I_x(\mathbf{e}_y) + I_x(\mathbf{e}_z) \sim \left| \left(\ddot{\mathbf{D}} \left(\mathbf{r}, t - \frac{s}{c} \right) \wedge \mathbf{e}_x \right) \wedge \mathbf{e}_x \right|^2$$

$$= |\ddot{\mathbf{D}} \cdot \mathbf{e}_y|^2 + |\ddot{\mathbf{D}} \cdot \mathbf{e}_z|^2, \quad (1)$$

where \mathbf{D} is the electric dipole moment, $\mathbf{r} = (x, y, z)$ is the location of the atom, \mathbf{e}_j ($j = x, y, z$) is the unit vector of j axis, and $I_x(\mathbf{e}_y)$ and $I_x(\mathbf{e}_z)$ are y - and z -polarized fluorescences along the x direction. An atom is subject to two external forces; the electric field force and Lorentz force. The electric field of the laser is $\mathbf{E} = \mathbf{E}_0 e^{-i\omega_L t + i\mathbf{K}_L \cdot \mathbf{r}} + \text{c.c.}$, and the quadrupole magnetic field near origin is [35]

$$B_x = \frac{b}{2}x, \quad B_y = \frac{b}{2}y, \quad B_z = -bz, \quad (2)$$

where b is the field gradient. The linear approximation of the magnetic field in Eq. (2) can hold at $\rho, |z| \leq 3$ cm in our experiment, with $\rho = \sqrt{x^2 + y^2}$ being the radial coordinate.

If considering only B_z , the result for the linearly polarized laser can be easily understood as a classical Hanle effect. As the oscillating plane of the electron precesses about the B_z direction with a Larmor frequency $\omega_z = \gamma B_z$ —where $\gamma = g(\mu_B/\hbar)$ is the gyromagnetic ratio, g the Landé factor

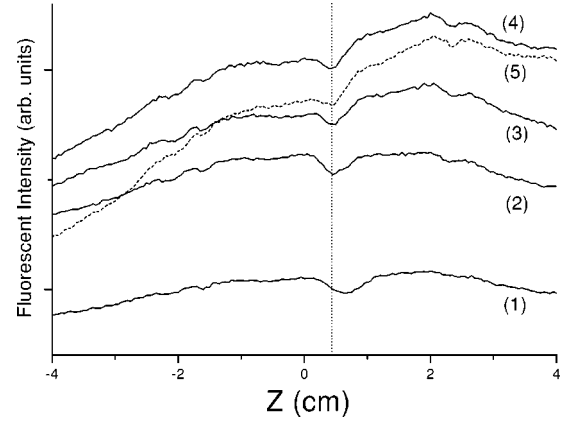


FIG. 6. The curves for unpolarized fluorescence under conditions of different detunings for $y \approx 0$ cm. (1) $\delta = 0$ MHz. (2) $\delta = -10$ MHz. (3) $\delta = -40$ MHz. (4) $\delta = -70$ MHz. (5) $\delta = -100$ MHz (dashed line).

(here taken to be $g = 1$) and $\mu_B = e\hbar/2m_e$ the Bohr magneton—the corresponding fluorescence intensity is given by

$$I_x \sim 1 - \frac{\Gamma^2/4}{\Gamma^2/4 + \omega_z^2}$$

for the π_x laser, and

$$I_x \sim 1 + \frac{\Gamma^2/4}{\Gamma^2/4 + \omega_z^2} \quad (3)$$

for the π_y laser, where Γ is the spontaneous decay rate of atom. The results illustrate that there is a dip for a π_x laser and a peak for a π_y laser at $z = 0$, just as we observed in experiment. However, we may run into some problem in the case of a circularly polarized laser. Since for a σ^+ laser, in a rotating frame (a frame rotating about the z axis at the laser frequency ω_L), an atom may “feel” a fictitious magnetic field $\tilde{B}_z = -\omega_L/\gamma$ in addition to the real field B_z , we may, in a reverse way, say that in the laboratory frame the atom is excited by a σ^+ laser with an effective frequency $\tilde{\omega}_L = \omega_L - \omega_z$ [36]. We can then easily obtain the steady-state y component of the dipole moment after a long enough time ($\sim 1/\Gamma$):

$$\mathbf{D} \cdot \mathbf{e}_y = \frac{e|\mathbf{E}_0|/m_e}{\sqrt{\Gamma^2 \tilde{\omega}_L^2 + (\omega_A^2 - \tilde{\omega}_L^2)^2}} \cos(\tilde{\omega}_L t + \theta). \quad (4)$$

As $\omega_z \ll \omega_L$ and $\omega_A \approx \omega_L$, we may take $\tilde{\omega}_L \approx \omega_L$ and $\omega_A^2 - \tilde{\omega}_L^2 \approx 2\omega_L(\omega_z - \delta)$, where $\delta = \omega_L - \omega_A$ is the detuning defined as the difference between the frequency of laser ω_L and that of L_3 transition ω_A . Therefore, from Eq. (4), the fluorescence can be derived:

$$I_x \sim \frac{1}{\Gamma^2/4 + (\omega_z - \delta)^2}. \quad (5)$$

If we take account of the atomic velocity, the detuning δ is replaced by $\delta_v = \delta - K_L v_z$. The total contribution from all velocity groups gives

$$I_x = \int I_x W(v_z) dv_z \sim \frac{\sqrt{\pi}}{iK_L} [Z(\Gamma/2 + i(\omega_z - \delta)) + Z(\Gamma/2 - i(\omega_z - \delta))], \quad (6)$$

where $W(v_z) = (1/\sqrt{\pi}u) e^{-(v_z/u)^2}$ is the Maxwell-Boltzman distribution, u is the most probable speed, and $Z(v)$ is the plasma dispersion function [37]. In the Doppler limit ($K_L u \gg \Gamma$), we have $Z(v) \approx i\sqrt{\pi} e^{-(\text{Im } v/K_L u)^2}$ and because $Z(v^*) = -Z^*(v)$, the fluorescence [Eq. (6)] then gives

$$I_x \sim e^{-[(\omega_z - \delta)/K_L u]^2}. \quad (7)$$

From Eq. (7), we can see that the decrease in the wings of the fluorescence distribution may be understood as due to the larger detuning induced by larger Zeeman splitting ω_z . But we may expect a peak rather than a dip at $z \approx 0$. Moreover, the z -polarized fluorescence $I_x(\mathbf{e}_z) \sim |\mathbf{D} \cdot \mathbf{e}_z|^2$ is always null. These two points are inconsistent with the experimental results for a circularly polarized laser.

It is known that some sources, such as saturation hole burning and optical pumping into a dark state decoupled to the laser, under the condition of a 1D inhomogeneous axial magnetic field, can result in a position-dependent fluorescence reduction. However, a careful study in Sec. IV shows that they are not relevant to the phenomenon. We found, through a qualitative argument, that in order to explain the experimental observation, we have to take into account the transverse or radial magnetic field. A physical picture can be constructed as follows: The radial magnetic field B_ρ induces a precession of the classical magnetic moment, associated with a magnetic dipole transition between Zeeman sublevels. As a direct result of this precession, a nonzero $I_x(\mathbf{e}_z)$ may be expected, and a peak in it may be assumed at $z=0$, because B_ρ , a dc field, will be on resonance when the Zeeman splitting is zero. In this simple picture, we can see that an increase of fluorescence in the z -polarized direction (corresponding to a π or $\Delta m=0$ emission, where m is the magnetic quantum number) occurs at the expense of a decrease in the y direction (corresponding to σ^\pm or $\Delta m = \pm 1$ emissions). More detailed features about the role played by B_ρ may require some more careful calculations to clarify.

Now we will treat the problem in detail by an approach of quantum mechanics. In the atomic rest frame, in conjunction with the electric-dipole and rotating-wave approximations, the systematic Hamiltonian can be written in the Heisenberg picture as

$$H = H_A + V_E + V_B,$$

$$H_A = \sum_{m,n} \hbar \omega_m^e \sigma_{mm}^{ee} + \hbar \omega_n^g \sigma_{nn}^{gg},$$

$$V_E = \sum_{m,n} \hbar \Omega_{mn}^{eg} \sigma_{nm}^{ge} e^{-i(\omega_L - K_L v_z)t} + \text{H.c.},$$

$$V_B = \sum_{m,m',n,n'} \hbar \Omega_{mm'}^{ee} \sigma_{m'm}^{ee} + \hbar \Omega_{nn'}^{gg} \sigma_{n'n}^{gg} + \text{H.c.}, \quad (8)$$

where H_A represents the free energy of atoms, and V_E and V_B are the interactions of atoms with the laser and the magnetic field, respectively. $\sigma_{nm}^{\alpha\beta} = |F_\beta, m\rangle \langle F_\alpha, n|$ is the atomic operator, $\Omega_{mn}^{eg} = \sum_{q=-1,0,1} \Omega_0 E_q C_{n-q,n}^{eg} \delta_{q,n-m}$ and $\Omega_{pp'}^{\alpha\alpha} = \gamma_\alpha \sum_{q=-1,0,1} B_{-q} C_{p,p-q}^{\alpha\alpha} \delta_{q,p-p'}$ are coupling coefficients, with $\Omega_0 = -d|\mathbf{E}_0|/\hbar$ the Rabi frequency, $d = \langle F_e || \mathbf{D} || F_g \rangle$ the reduced matrix element, $E_q = \mathbf{E}^{(+)} \cdot \mathbf{e}_q^*$ the polarized component of the classical laser electric field, $\mathbf{e}_{\pm 1} = \mp (1/\sqrt{2})(\mathbf{e}_x \pm i\mathbf{e}_y)$, $\mathbf{e}_0 = \mathbf{e}_z$, $C_{p,p-q}^{eg}$ the Clebsch-Gordan coefficient, $\gamma_\alpha = g_\alpha \gamma$ the gyromagnetic ratio for hyperfine level F_α and g_α the effective Landé factor of F_α in the weak-magnetic-field regime ($g_e = 2/3$ for $F_e = 0, 1, 2$, and 3 and $g_g = 1/2$ for $F_g = 2$). $B_{\pm 1} = (1/\sqrt{2})(B_x \pm iB_y)$ and $B_0 = B_z$ are components of the magnetic field, and $C_{p,p-q}^{\alpha\alpha} = (1/\sqrt{2})|q| \sqrt{F_\alpha(F_\alpha+1) - p(p-q)} + (1-|q|)p$ represents the strength of the magnetic dipole moment transition. Further taking account of the coupling with the vacuum field and after elimination of the bath operators [37], we can obtain the optical Bloch equations (OBE's), which give the evolution of the atomic density operator $\rho_{pp'}^{\alpha\beta} = \langle \sigma_{pp'}^{\alpha\beta} \rangle$,

$$\frac{d}{dt} \rho_{pp'}^{\alpha\beta} = \frac{d^{(1)}}{dt} \rho_{pp'}^{\alpha\beta} + (\rho_{pp'}^{\alpha\beta})_f + \frac{i}{\hbar} \langle [H, \sigma_{pp'}^{\alpha\beta}] \rangle, \quad (9)$$

where $d^{(1)}/dt$ denotes the relaxation of excited states, optical coherence, and the repopulation of ground states with

$$\begin{aligned} \frac{d^{(1)}}{dt} \rho_{mm'}^{ee} &= -\Gamma \rho_{mm'}^{ee}, \\ \frac{d^{(1)}}{dt} \rho_{mn}^{eg} &= -\frac{\Gamma}{2} \rho_{mn}^{eg}, \end{aligned} \quad (10)$$

$$\frac{d^{(1)}}{dt} \rho_{nn'}^{gg} = \Gamma \sum_{q=-1,0,1} C_{n+q,n}^{eg} C_{n'+q,n'}^{eg} \rho_{n+q,n'+q}^{ee}.$$

In Eq. (10), we have taken the spontaneous emission rates of excited states to be equal ($\Gamma = 2\pi \times 6$ MHz for ^{87}Rb), and neglected the relaxation related to the interatomic collisions, since the mean length of free path is by far beyond the magnitude of the vacuum cell under the experimental vapor pressure. $(\rho_{pp'}^{\alpha\beta})_f$ represents the coherence between states due to the vacuum field coupling, for example,

$$(\rho_{mm}^{ee})_f = - \sum_{m',e'} K_{mm'}^{ee'} \rho_{m'm}^{e'e} + \text{H.c.}, \quad (11)$$

$$K_{mm'}^{ee'} = \sum_{f,g} \frac{\pi \omega_f}{2\epsilon_0 \hbar V} G_{mm'}^{ee'}(\mathbf{e}_f) \delta(\omega_f - \omega_{e'g}) e^{i\omega_{mm'}^{ee'} t},$$

where $\omega_{mm'}^{ee'}$ is the energy separation between excited states $|F_e, m\rangle$ and $|F_{e'}, m'\rangle$. $G_{mm'}^{ee'}(\mathbf{e}_f)$ is the emission matrix element, with

$$G_{mm'}^{ee'}(\mathbf{e}_f) = \langle F_e, m | \mathbf{e}_f \cdot \mathbf{D} | F_g, n \rangle \langle F_{e'}, m' | \mathbf{e}_f \cdot \mathbf{D} | F_g, n \rangle^*, \quad (12)$$

where \mathbf{e}_f is the unit vector for electric field of vacuum field propagating in a direction (ϕ_f, θ_f) (polar coordinates) with a polarization α_f and frequency ω_f , and

$$\mathbf{e}_f \cdot \mathbf{D} = \sum_{q=-1,0,1} (-1)^q \xi_{-q} |C_{n+q,n}^{eg}| \sigma_{nm}^{ge} \delta_{m,n+q}, \quad (13)$$

$$\xi_{-q} = \frac{1}{\sqrt{2}} q (\cos \theta_f \cos \alpha_f - iq \sin \alpha_f) e^{-iq\phi_f}$$

$$+ (|q| - 1) \sin \theta_f \cos \alpha_f.$$

The term $(\rho_{pp'}^{\alpha\beta})_f$ will cause a SPI in fluorescence, while since $\omega_{mm'}^{ee'}$ in our case is always much larger than the natural level width Γ , the coherence can be ignored.

The scattered field intensity emitted in a solid angle (ϕ_f, θ_f) , with a polarization α_f [for I_x , $\phi_f=0$ or π , $\theta_f = \pi/2$ and for $I_x(\mathbf{e}_y)$, $\alpha_f = \pi/2$, for $I_x(\mathbf{e}_z)$, $\alpha_f=0$], is given by

$$I_f = \frac{3N\Gamma}{8\pi|d|^2} \sum_{m,m'} G_{mm'}^{ee} \rho_{m'm}^{ee}, \quad (14)$$

where $G_{mm'}^{ee} = \sum_{g,n} G_{mm'}^{eg}(\mathbf{e}_f)$, and N is the atomic density at \mathbf{r} . The population and Zeeman coherence of excited state $\rho_{m'm}^{ee}$ can be obtained from the OBE (9). In order to provide a physical picture, instead of a more complex $F_g=2 \rightarrow F_e=3$ transition, we turn to a simplified model, with which an analytical expression for I_f may be obtained. We adopt the multilevel model $J_g=1/2 \rightarrow J_e=3/2$, which may be the simplest one to approximate the real system (since we should consider the magnetic moment precession, a two-level model is invalid, and a model $J_g=0 \rightarrow J_e=1$ will exclude the ground-state precession which may be especially important for low laser powers).

We may diagonalize the coupling with magnetic field in Eq. (8) by transforming the system from a z representation to a B representation where the axis of quantization is chosen along the local direction of the magnetic field. The transformation operator is given by

$$U = e^{iJ_y \theta_B / \hbar} e^{iJ_z \phi / \hbar}, \quad (15)$$

where $\theta_B = \cos^{-1}(B_z/B)$, $\phi = \tan^{-1}(y/x)$, $B = \sqrt{B_z^2 + B_\rho^2}$, and $B_\rho = \sqrt{B_x^2 + B_y^2}$ is the strength of radial magnetic field. The OBE in the new representation takes a form

$$\frac{d}{dt} \tilde{\rho}^{\alpha\beta} = \frac{d^{(1)}}{dt} \tilde{\rho}^{\alpha\beta} + \frac{i}{\hbar} [\tilde{\rho}^{\alpha\beta}, \tilde{H} + H_v], \quad (16)$$

where $d^{(1)}/dt$ has the same form as Eq. (10), as it is isotropic and independent of the axis of quantization. $\tilde{\rho}^{\alpha\beta} = U \rho^{\alpha\beta} U^\dagger$ is the new density matrix,

$$U = \begin{pmatrix} U_e & 0 \\ 0 & U_g \end{pmatrix},$$

and U_e and U_g are corresponding transformations for excited and ground states. $\tilde{H} = U H U^\dagger = H_A + \tilde{V}_E + \tilde{V}_B$,

$$\tilde{V}_B = \begin{pmatrix} \gamma_e J_z B & 0 \\ 0 & \gamma_g J_z B \end{pmatrix} \quad \text{and} \quad \tilde{V}_E = \begin{pmatrix} 0 & \tilde{\Omega} \\ \tilde{\Omega}^* & 0 \end{pmatrix}$$

with ,

$$\tilde{\Omega} = U_e \Omega U_g^\dagger, \quad (17)$$

$$\Omega = \text{Tr} \begin{pmatrix} 0 & 0 & 0 & \Omega_{3/2,1/2}^{eg} \\ 0 & 0 & \Omega_{1/2,-1/2}^{eg} & 0 \end{pmatrix}.$$

$\tilde{\Omega}$ is a transformed Rabi frequency in the B representation. H_v is an extra potential depending on the atom velocity induced by the unitary transformation in the new Hamiltonian,

$$H_v = \frac{xv_y - yv_x}{\rho^2} (J_x \sin \theta_B - J_z \cos \theta_B) + \frac{zv_\rho - \rho v_z}{4z^2 + \rho^2} J_y, \quad (18)$$

corresponding to the nonadiabatic evolution of atomic operators. Because the magnetic field is space dependent, a moving atom may feel in its rest frame that the external magnetic field keeps changing. Thus the density operators should be velocity dependent and $(d/dt)\rho^{\alpha\beta}(\mathbf{r}, \mathbf{v}, t) = (\partial/\partial t)\rho^{\alpha\beta} + \mathbf{v} \cdot \nabla \rho^{\alpha\beta}$. This means that a time-dependent solution is needed. Unfortunately, a strict solution of this kind is usually unavailable. If the magnetic field changes very slowly during an interval from a time $t - \Delta t$ when an atom is excited by a magnetic field to a time t when a steady state can be obtained, we may take the magnetic field to be constant during the interval and obtain a stationary solution by neglecting the term $\mathbf{v} \cdot \nabla \rho^{\alpha\beta}$ and H_v . This slowly varying condition can be expressed as $\Delta B \ll B$ in Δt . As Δt is of the order of the optical pumping time $1/\Gamma_p$, the condition can be reexpressed as $|\mathbf{v}|/\Gamma_p \ll \rho, |z|$, or in other words, the condition cannot hold at a region ρ , or $|z| \leq |\mathbf{v}|/\Gamma_p$. It can be seen that the larger the optical pumping rate Γ_p (proportional to laser power) is, the smaller the region is. This is because the circularly polarized laser will act like a bias magnetic field along the z axis, preventing a nonadiabatic (Majorana) spin-flip. Taking $|\mathbf{v}|$ to be the most probable speed $u \sim 10^3$ m/s at 300 K and $\Gamma_p \sim 10^7$ /s, we have $|\mathbf{v}|/\Gamma_p \sim 0.01$ cm, which is much smaller than the half-width of dark region. In fact, in the experiment we have used a sheetlike laser beam with a thickness of 1–2 mm instead of one with a round section, and changed the incident position along the x axis. The observation is similar to those in Fig. 2 and the dip is even darker for larger x . Therefore the nonadiabatic evolution is not essential for an understanding of the phenomenon. In the following we will first give a stationary solution of the OBE under an adiabatic approximation, and then consider the effect of nonadiabatic evolution.

A. Adiabatic approximation

In the region $\rho, |z| \gg |\mathbf{v}|/\Gamma_p$, we can omit the velocity-dependent operators H_v and $\mathbf{v} \cdot \nabla \rho^{\alpha\beta}$. When the laser power is low so that the Rabi frequency Ω_0 is much smaller than the decay rate Γ , the optical coherence $\tilde{\rho}^{eg}$ will be small, and can be expressed, to first order in $\tilde{\Omega}^{eg}$, for example, as

$$\tilde{\rho}_{3/2,1/2}^{eg} = \frac{-i\tilde{\Omega}_{3/2,1/2}^{eg}\tilde{\rho}_{1/2,1/2}^{gg}e^{-i(\omega_L - K_L v_z)t}}{\Gamma/2 - i(\delta_v - \omega_{3/2,1/2}^{eg})}, \quad (19)$$

where $\omega_{pp'}^{\alpha\beta} = (g_\alpha p - g_\beta p')\omega_B$, and $\omega_B = \gamma B$ is the Larmor precession frequency around the local magnetic field. In terms of the expressions of $\tilde{\rho}^{eg}$, we can adiabatically eliminate the populations and the coherence of excited states $\tilde{\rho}^{ee}$, which can be written as

$$\tilde{\rho}_{mm'}^{ee} = \frac{\sum_{nn'} P_{mm'}^{nn'} \tilde{\rho}_{nn'}^{gg}}{\Gamma + i(m - m')g_e \omega_B}. \quad (20)$$

Here $P_{mm'}^{nn'}$ is the excitation matrix, with

$$\begin{aligned} P_{mm'}^{nn'} &= \Omega_{mm'}^{nn'} (T_{m'n} + T_{mn'}^*), \\ \Omega_{mm'}^{nn'} &= \tilde{\Omega}_{m/2, n/2}^{eg} (\tilde{\Omega}_{m'/2, n'/2}^{eg})^*, \\ T_{mn} &= \frac{1}{\Gamma/2 + i(\delta_v - \omega_{m/2, n/2}^{eg})}. \end{aligned} \quad (21)$$

On the basis of Eqs. (20) and (21), we can obtain a closed set of equations for ground-state density operators $\tilde{\rho}^{gg}$. The calculation is straightforward (the result is rather lengthy and will be given elsewhere). From the stationary solution for $\tilde{\rho}^{gg}$, we can give ρ^{ee} in the z representation:

$$\rho_{mm'}^{ee} = \sum_{m'', m''', n, n'} \frac{(U_e^+)_{mm''} P_{m''m'''}^{nn'} \tilde{\rho}_{nn'}^{gg} (U_e^-)_{m''m'm'}}{\Gamma + i(m'' - m''')g_e \omega_B}. \quad (22)$$

Inserting Eq. (22) into Eq. (14), we can obtain I_f . We further integrate Eq. (14) over the distribution of v_z and x , i.e., $\int_{-\sqrt{R^2 - y^2}}^{\sqrt{R^2 - y^2}} dx$, with R the radius of the laser beam (the nonadiabatic evolution region may be treated as a singular point and removed from the integral). A numerical calculation shows that the value of I_f at $z \approx 0$ is mainly determined by the velocity components around $v_z = \delta/K_L$. This is not surprising, because those groups with $\delta_v \gg \Gamma$ near the origin will cause a large effective detuning $\delta_v - \omega_{mn}^{eg}$, and the corresponding $\tilde{\rho}^{ee}$ will be small and lead to a weak fluorescence. This fact may also explain why the location of the dip center is not sensitive to the laser frequency scanning. In Fig. 7, we

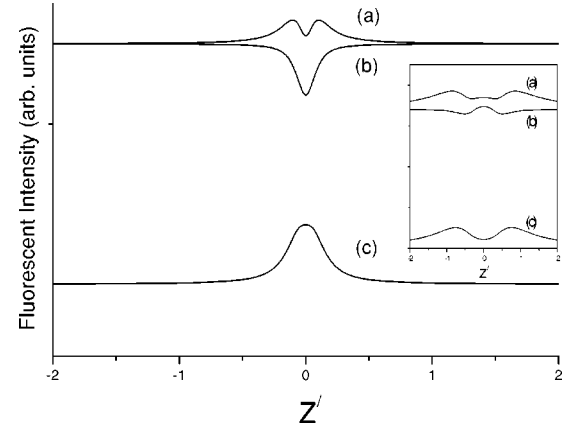


FIG. 7. The theoretical curves for x -directional fluorescence vs z coordinates with dimensionless parameters $z' = \gamma b z / \Gamma$, $R' = \gamma b R / \Gamma = 0.5$, $y' = \gamma b y / \Gamma = 0$, $\delta' = \delta / \Gamma = 0$, and $\Omega'_0 = \Omega_0 / \Gamma = 0.3$. (a), (b), and (c) have the same meaning as in Fig. 2. $\Omega'_0 = 5$ for the curves in the inset.

plot a result for certain parameters with Landé factors $g_e = 4/3$ for $J_e = 3/2$ and $g_g = 2$ for $J_g = 1/2$. We can see that the theoretical curve can recover the experimental observation qualitatively. Moreover, we have found that for a sufficiently large radial coordinate ρ , the peak in z -polarized fluorescence will split into two peaks with a minimum at $z = 0$ (see Fig. 8). This result is actually the so-called saturation of magnetic resonance already known in double-resonance experiments, because the large magnetic precession can substantially reduce the population difference between excited states in their lifetime. In the experiment, we have observed a bright X-shaped region across the beam in $I_x(\mathbf{e}_z)$, which was more apparent for lower laser intensities (where the radial magnetic field will seem to be relatively larger). On the other hand, when the laser power is very high, $\tilde{\rho}^{ee}$ become significant, and we have to solve the model strictly without the low-power assumption. A similar result can be obtained, but the dip in unpolarized, or y -polarized fluorescences or the peak in z -polarized fluorescence will become much shallower or flatter with increasing laser intensity (for a high enough laser power, the dip will even be inverted to a peak and the peak to a dip; see the inset of Fig. 7).

In order to provide some insight into the phenomenon, an

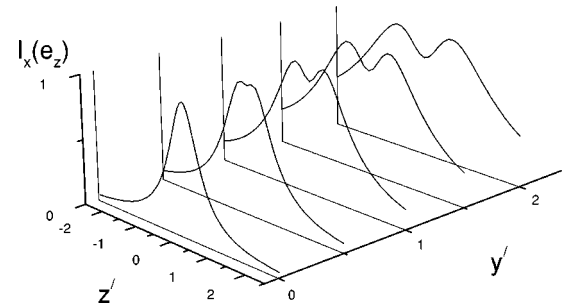


FIG. 8. The theoretical variations of the z -polarized fluorescence distribution (normalized) for different distances from the z axis with $x = 0$, $\delta' = 0$, and $\Omega'_0 = 0.3$, where the parameters are dimensionless ones defined in Fig. 7.

analytic expression for I_f with variables of clear physical meanings may be helpful. In the above method, we initially transform the system to a B representation and then study the interaction of the magnetic-field dressed atom with the laser field. The final expression [Eq. (22)] is complicated and hard to picture simply, partly because in a B representation a σ^+ laser will excite σ^+ , σ^- , and π transitions. In the following, we further simplify the solution of OBE (16), in the regime of weak laser power, by studying the problem in a reverse way; that is, first dressing the atom with the laser field and then considering the interaction of a laser-dressed ground state with a magnetic field in the z representation, with an assumption that the coherence between sublevels of the excited state is negligible. In this picture, the free energy of the ground state can be replaced by the light shifts $\Delta_{-1/2}$ and $\Delta_{1/2}$, with

$$\Delta_{-1/2} = \frac{2}{3}\Delta, \quad \Delta_{1/2} = 2\Delta, \quad \Delta = \delta_v s_0, \quad (23)$$

where s_0 is the saturation parameter:

$$s_0 = \frac{|\Omega_0|^2/2}{\Gamma^2/4 + \delta_v^2}. \quad (24)$$

The reduced Hamiltonian is then given by

$$\bar{H} = \begin{pmatrix} \Delta_{-1/2} - \frac{1}{2}g_g\omega_B & \frac{1}{2}g_g\omega_\rho e^{i\phi} \\ \frac{1}{2}g_g\omega_\rho e^{-i\phi} & \Delta_{1/2} + \frac{1}{2}g_g\omega_B \end{pmatrix}, \quad (25)$$

where $\omega_\rho = \gamma B_\rho$ is the precession frequency due to the radial magnetic field. The depopulation and repopulation of ground states can be easily obtained as

$$\frac{d^{(1)}}{dt}\rho^{gg} = \begin{pmatrix} -\frac{\Gamma_p}{3}\rho_{-1/2,-1/2}^{gg} & -\frac{2\Gamma_p}{3}\left(1 - i\frac{\delta_v}{\Gamma}\right)\rho_{-1/2,1/2}^{gg} \\ -\frac{2\Gamma_p}{3}\left(1 + i\frac{\delta_v}{\Gamma}\right)\rho_{1/2,-1/2}^{gg} & -\Gamma_p\rho_{1/2,1/2}^{gg} \end{pmatrix}, \quad (26)$$

$$\frac{d^{(2)}}{dt}\rho^{gg} = \begin{pmatrix} \frac{\Gamma_p}{9}\rho_{-1/2,-1/2}^{gg} & \frac{\Gamma_p}{3}\rho_{-1/2,1/2}^{gg} \\ \frac{\Gamma_p}{3}\rho_{1/2,-1/2}^{gg} & \frac{2\Gamma_p}{9}\rho_{-1/2,-1/2}^{gg} \end{pmatrix},$$

where $\rho^{gg} = (\rho_{nn}^{gg})_{2 \times 2}$ is the ground-state density matrix, and $\Gamma_p = \Gamma s_0$ is the optical pumping rate. The evolution of ρ^{gg} takes a form

$$\frac{d}{dt}\rho^{gg} = \left(\frac{d^{(1)}}{dt} + \frac{d^{(2)}}{dt}\right)\rho^{gg} + \frac{i}{\hbar}[\rho^{gg}, \bar{H}]. \quad (27)$$

We can reexpress Eq. (27) in a more classical form in terms of the magnetic moment,

$$\frac{d}{dt} \begin{pmatrix} M_x \\ M_y \\ M_z \end{pmatrix} = \begin{pmatrix} -\frac{\Gamma_p}{3} & -2\Delta - g_g\omega_z & g_g\omega_\rho \sin \phi \\ 2\Delta + g_g\omega_z & -\frac{\Gamma_p}{3} & -g_g\omega_\rho \cos \phi \\ -g_g\omega_\rho \sin \phi & g_g\omega_\rho \cos \phi & -\frac{2\Gamma_p}{9} \end{pmatrix} \begin{pmatrix} M_x \\ M_y \\ M_z \end{pmatrix} + \begin{pmatrix} 0 \\ 0 \\ \frac{2\Gamma_p}{9} \end{pmatrix}, \quad (28)$$

where M_x , M_y , and M_z are components of the magnetic moment of the atomic ensemble, defined as $M_x = \rho_{1/2,-1/2}^{gg} + \rho_{-1/2,1/2}^{gg}$, $M_y = i(\rho_{1/2,-1/2}^{gg} - \rho_{-1/2,1/2}^{gg})$, and $M_z = \rho_{1/2,1/2}^{gg} - \rho_{-1/2,-1/2}^{gg}$. In deriving Eq. (28) we have used the normalization relation $\rho_{1/2,1/2}^{gg} + \rho_{-1/2,-1/2}^{gg} = 1$. On the other hand, the fluorescence intensity will also obtain simple forms:

$$I_x(\mathbf{e}_y) = \frac{N\Gamma_p}{4\pi} \left(\frac{5}{4} + M_z \right),$$

$$I_x(\mathbf{e}_z) = \frac{N\Gamma_p}{8\pi} (1 - M_z), \quad (29)$$

$$I_x = I_x(\mathbf{e}_y) + I_x(\mathbf{e}_z) = \frac{N\Gamma_p}{8\pi} \left(\frac{7}{2} + M_z \right).$$

We can obtain a stationary solution of Eq. (28):

$$M_z = 1 - \frac{3\omega_\rho^2}{2\left(\frac{\Gamma_p}{6}\right)^2 + 2(\Delta + \omega_z)^2 + 3\omega_\rho^2}. \quad (30)$$

Equation (30) shows that for nonzero ω_ρ , M_z has a reverse Lorentzian shape with respect to z , and is centered at $z_d = -\Delta/\gamma b \approx 0$ for a low saturation parameter $s_0 \ll 1$, where the largest $|z_d|$ is $|\Omega_0|^2/2\gamma b\Gamma$, occurring at a velocity $v_z = (\delta \pm \Gamma/2)/K_L$. Consequently, the fluorescences I_x , $I_x(\mathbf{e}_y)$, and $I_x(\mathbf{e}_z)$ obtain the profiles that we have observed in experiment. If $\omega_\rho = 0$, then there will be no dip. This is the same conclusion as that drawn from the classical model. Additionally, one may note that, from Eq. (30), a bimodal structure cannot be deduced in $I_x(\mathbf{e}_z)$ like that shown in Fig. 8. This is because that in the derivation we have neglected the magnetic precession in the excited state; this is equivalent to assuming $g_e = 0$, while the bimodal structure is a direct consequence of nonzero g_e .

Since M_z represents the orientation of the atom ensemble, one can infer, from Eqs. (29) and (30), that the dip in I_x is actually caused by a deorientation due to a radial precession which reaches its maximum near the point of level crossing $z=0$. From Eqs. (29) and (30), we can estimate the half-width (W) and contrast (C) of the dip,

$$W(\text{half-width}) = \frac{1}{6} \sqrt{\rho_c^2 + 54\rho^2}, \quad (31)$$

$$C(\text{contrast}) = \frac{27\rho^2}{\rho_c^2 + 27\rho^2}, \quad (32)$$

$$\rho_c = \frac{2\Gamma_p}{\gamma b},$$

where ρ_c is a characteristic distance at which the optical pumping rate is equal to the Larmor precession frequency. It can be seen that however, when $\rho \ll \rho_c$, the dip is inconspicuous, however; when $\rho \sim \rho_c$, the dip will be significant. As Γ_p is proportional to the laser intensity, expressions (31)

and (32) can very well explain the experimentally observed widening of the half-width with increasing laser intensity, and the decrease of the half-width and the saturation of the contrast for larger magnetic-field gradients. They may also explain why it is hard to observe a dip when the diameter of the laser beam is too small. As we know, the finite time it takes an atom to pass through a laser field will induce a time-of-flight broadening [27] that is equivalent to a relaxation rate $\Gamma' = 1/T$ (T is the crossing time) into the OBE (28) [23]: $\Gamma \rightarrow \Gamma + \Gamma'$ and $(d/dt)M_j = -\Gamma' M_j$. Therefore, the thinner a laser beam is, the smaller T is and the larger the effective Γ_p is. Consequently, the half-width will be larger and the contrast smaller.

However, although the above physical picture can qualitatively recover most of the experimental facts, we still have two points which may not be very well explained by the above two methods. The first is the variation of the contrast versus the laser intensity. While the experimental data indicate a contrary tendency, our simplified model shows that the contrast for the dip or peak should decrease with increasing laser intensity for either low laser power [see Eq. (32)] or high laser power. The theoretical tendency can be interpreted in the following manner: For high laser power, the precession effect will become relatively weak because of the strong optical pumping; in other words, as the light shift becomes large, the effective energy separation between Zeeman sublevels is greatly expanded and consequently, the coherence between these sublevels, which are coupled by the radial magnetic field B_ρ , reduces. This is equivalent to letting $B_\rho \rightarrow 0$. Therefore, we could expect the dip and peak in I_x , whose modification is determined by B_ρ , to eventually disappear. The second tendency, which is less important, is the asymmetry accompanied with the detuning. Although it shows that detuning does not affect the location of the dip, the theory tells us that a significant asymmetry should occur only at a very large detuning (δ larger than about 40Γ), while in the experiment the requirement for such a δ is much smaller (see Fig. 6). Both these problems will be discussed in Sec. IV, where we propose that the nonvanishing contrast may be due to of the presence of other hyperfine transitions, and some of the asymmetry is attributed to the hole burning and population loss to the lower hyperfine level.

B. Effect of nonadiabatic evolution

In the above calculations, we have used an assumption of small Γ_p . As analyzed above, this may result in a large nonadiabatic evolution region. One may therefore need to consider its effect at the place of small ρ and z .

By using variable transformations

$$M_\rho = \frac{M_x \cos \phi + M_y \sin \phi}{2}, \quad M_\phi = \frac{M_x \sin \phi - M_y \cos \phi}{2}, \quad (33)$$

OBE (28) can be made free of ϕ , and re-expressed as

$$\frac{d}{dt}M = (A_0 + bA_1)M + C, \quad (34)$$

$$A_0 = \begin{pmatrix} -\frac{\Gamma_p}{3} & 2\Delta - \phi & 0 \\ \phi - 2\Delta & -\frac{\Gamma_p}{3} & 0 \\ 0 & 0 & -\frac{2\Gamma_p}{9} \end{pmatrix},$$

$$A_1 = \begin{pmatrix} 0 & \gamma_g z & 0 \\ -\gamma_g z & 0 & \frac{1}{4}\gamma_g \rho \\ 0 & -\gamma_g \rho & 0 \end{pmatrix},$$

$$C = \text{tr} \begin{pmatrix} 0 & 0 & \frac{2\Gamma_p}{9} \end{pmatrix}, \quad M = \text{tr}(M_\rho \ M_\phi \ M_z),$$

where $\dot{\phi} = d\phi/dt$ is the angular frequency of the atomic motion. As the magnetic-field gradient is a small parameter in our experiment ($\gamma b\rho/\Gamma, \gamma b|z|/\Gamma \ll 1$ the near origin), we can use a perturbation method to solve the velocity-dependent OBE (34). Expanding the density matrix in b

$$M = M_0 + bM_1 + b^2M_2 + \dots, \quad (35)$$

substituting Eq. (35) into Eq. (34) and equating the coefficients of order b^n , we obtain

$$\frac{d}{dt}M_n = A_0M_n + C_n, \quad (36)$$

$$C_0 = C, \quad C_n = A_1M_{n-1}.$$

A time-dependent formal solution of the recursive differential equation (36) can be written as

$$M_n(t) = e^{A_0(t-t_0)}M_n(t_0) + \int_{t_0}^t e^{A_0(t-t')}A_1(t')M_{n-1}(t')dt'. \quad (37)$$

Supposing the atoms are initially in the state $|J_g, m=1/2\rangle$ before the quadrupole magnetic field is switched on, that is,

$$M_0(t_0) = \text{tr}(0 \ 0 \ 1), \quad M_{n \neq 0}(t_0) = 0, \quad (38)$$

substituting

$$z(t') = z(t) + v_z(t' - t), \quad \rho(t') = \rho(t) + v_\rho(t' - t), \quad (39)$$

for $z(t')$ and $\rho(t')$ in $A_1(t')$, and taking $t_0 \rightarrow -\infty$, we can calculate the integral in Eq. (37). What we are interested in is the expression for M_z , which can be simplified if taking $\phi - 2\Delta \approx 0$ (see the Appendix), and we have

$$M_z \approx \frac{486\gamma^4 b^4}{\Gamma_p^6} (\Gamma_p \rho - 9v_\rho)^2 z^2 + b^4 a_{41} z + b^2 a_{20} + 1. \quad (40)$$

Since the coefficient of z^2 in Eq. (40) is always positive for $v_\rho \neq \Gamma_p \rho/9$, the curve of M_z versus z will be of a parabolic shape with its minimum near $z=0$. Therefore, including the velocity dependency will not change the qualitative result we obtained in Sec. II A. Equation (40) also indicates that even for $\rho=0$, M_z has a dip due to the existence of v_ρ . The velocity in Eq. (40) actually represents the deorientation of the atom ensemble induced by nonadiabatic evolution.

IV. DISCUSSION

A. Coherent population trap

In terms of a classical concept—i.e., the precession of the magnetic moment—in Sec. III, we qualitatively explained the origin of the central dark region. Here we will argue that this phenomenon can be understood, from another point of view, as a result of a destructive quantum interference effect in the presence of two fields: one is a laser field, the other is a radial magnetic field which couples Zeeman sublevels. The interaction of an atom, whose level is shifted by the axial magnetic field, with these two fields can be treated in much the same way as the coherent double-quantum transition considered in Refs. [6–24].

Before going any further, we first want to answer a possible question, that is, whether the decrease in fluorescence along the observation direction is only a destructive quantum interference in certain directions as in the classical Hanle effect, or is caused by a population trap. We find the phenomenon is actually the latter. If we sum over all radiation directions and polarizations, we obtain the total fluorescence in terms of M_z in Sec. III:

$$I_{total} = \sum_{\alpha_f} \int I_f \sin \theta_f d\theta_f d\phi_f = \frac{N\Gamma_p}{2} (2 + M_z). \quad (41)$$

This indicates that there is also a dip around the zero-field point in total fluorescence. This means that the phenomenon is not just a result of a partial selection of final states. Equation (41) can be understood as a result of a CPT for a V-type construction which is composed of two ground states $|J_g, m = \pm 1/2\rangle$ and an excited state $|J_e, m = 3/2\rangle$, coupled by both a radial magnetic field and a light field. Treating $\Omega_0, \gamma_g B_\rho, |J_e, m = J_e\rangle, |J_g, m = J_g - 1\rangle$, and $|J_g, m = J_g\rangle$ as $\beta_1, \beta_2, |3\rangle, |2\rangle$, and $|1\rangle$ in Ref. [15], respectively, the problem can be readily transformed to what has been discussed therein. Reference [15] showed that atoms may be trapped in some dressed states; when these dressed states are mainly composed of two ground levels $|2\rangle$ and $|1\rangle$, e.g., in the limit of very strong β_2 and weak β_1 , a great decrease in fluorescence will occur. Reference [15] also illustrated that when increasing β_1 with β_2 fixed, more and more atoms will be trapped in states $|3\rangle$ and $|1\rangle$. This means that the modification in fluorescence caused by the population in state $|2\rangle$, which accounts for the increase in $I_x(\mathbf{e}_z)$ and the decrease in

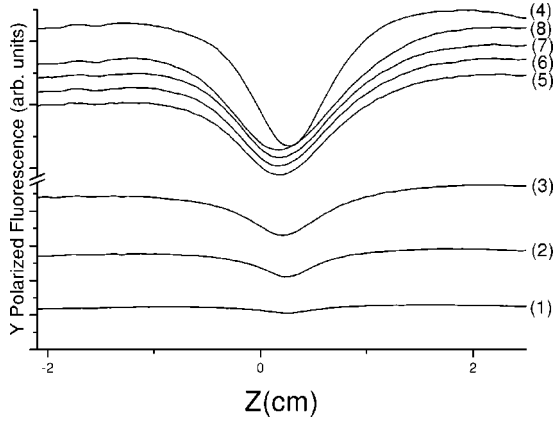


FIG. 9. The experimental curves of the y -polarized fluorescence in the x direction for different laser intensities with beam diameter 1.5 cm, coil current 2.5 A, $y \approx 0$ cm and at near resonance. (1) 0.6 mW cm^{-2} . (2) 2 mW cm^{-2} . (3) 9 mW cm^{-2} . (4) 18 mW cm^{-2} . (5) 29 mW cm^{-2} . (6) 43 mW cm^{-2} . (7) 50 mW cm^{-2} . (8) 59 mW cm^{-2} .

$I_x(\mathbf{e}_y)$, will reduce, and the contrast should be consequently smaller. This is just what Eqs. (32) and (41) have told us. For a high laser power, where the population of excited states cannot be neglected and atoms stay mainly in one sublevel of the ground state because of the strong optical pumping (i.e., $\Gamma_p \gg \omega_B$), we can have a Λ -type system composed of $|J_g, m=1/2\rangle$ and $|J_e, m=1/2, 3/2\rangle$, with two coupling fields. These schemes, although not perfectly closed, will be enough for an estimation of the quantum interference produced both in certain directional fluorescence and in total fluorescence. If we dress the two excited states with a radial magnetic field, the above Λ -type system can be transformed to the SPI-like scheme which has received wide investigation [6,10,11]. This scheme shows that, since the effective dipole moments for the respective transitions from two dressed upper states to the lower state are not parallel (as there is only one metastable state in the Λ -type system), the destructive quantum interference will not cause a total suppression, and more importantly, will actually disappear for high laser power [6]. This is consistent with the analysis given at the end of Sec. III A. In addition, there is another kind of V -type CPT found when considering a weak reflection of a laser by a chamber window, which can form a standing wave. As a moving atom will experience a bichromatic field in its rest frame, for those atoms with suitable velocities [20] at the same place of the crossover hole (given in Sec. IV C), the maximum two-photon coherence condition [15,19] can be achieved in a V -type scheme, which comprises transitions $|F_g, m-1\rangle \rightarrow |F_e = F_g, F_g \pm 1, m\rangle$. Unfortunately, unlike Ref. [20], which used a third laser, here we cannot separate this V -type CPT from the crossover hole in space.

In Sec. III, it was shown that, according to the theory, the contrast of the dip in unpolarized fluorescence should die out with increasing laser intensity. But this tendency is in contradiction to the experimental data. In addition, in the experiment we have recorded the variations of y - and z -polarized fluorescences with increasing laser intensity. From Fig. 9, it can be seen that the dip in $I_x(\mathbf{e}_y)$ [and also the corresponding

peak in $I_x(\mathbf{e}_z)$, not shown in the figure] is still apparent for high laser powers. However, the above analysis has shown that the $F_g = 2 \leftrightarrow F_e \leftrightarrow F_g = 2$ system cannot account for this result. The reason for these contradictions is not yet very clear. One possible explanation is that when the laser intensity is high (the saturation intensity for the $^{87}\text{Rb } D_2$ line is about 2.6 mW cm^{-2}), the large power broadening of lines will allow not only a single transition $F_e - F_g = 1$ even for small detunings; thus the closed transition model used in Sec. III will become invalid because atoms can be pumped to the lower hyperfine level $F_g = 1$ for a $F_g \rightarrow F_e \leq F_g$ transition. The spontaneous emission rate Γ for the σ - and π -polarized fluorescences in the theoretical treatment should be replaced by $\Gamma/(1 + \alpha)$ for the open transition [22], where $\alpha = \Gamma_{F_e \rightarrow F_g = 1} / \Gamma_{F_e \rightarrow F_g = 2}$ is the ratio between different spontaneous decays, since atoms in $F_g = 1$ do not contribute to the fluorescence. The reduced effective spontaneous emission rate may cancel the increase in the laser intensity, and result in the effective optical pumping rate not increasing, and consequently the contrast not decreasing, synchronously with the variation of the laser power [38].

B. Scattering-path-interference by vacuum-field coupling

Besides the CPT, there may be another kind of quantum interference phenomenon, i.e., SPI, as indicated in Sec. I. We can see that, in the presence of a traveling σ^+ laser, a ground sublevel $|F_g = 2, m-1\rangle$ can be coherently excited to $|F_e = 1, 2, 3, m\rangle$, and establish a destructive SPI scheme, since the dipole moments $\langle F_e, m | \mathbf{D} | F_g, m-1 \rangle$ for the transitions are parallel. However, since the bare excited states are coupled only by a vacuum field [see Eq. (11)], a considerable SPI requires that the energy separation of two states be smaller than the natural width of the excited state. However, we note the separation of these excited states $\Delta_{13}, \Delta_{23}, \Delta_{21} \gg \Gamma$; therefore, the SPI caused by vacuum field coupling in our case can be ignored.

C. Saturation hole burning

We have already discussed above the quantum interference effects in the system. However, it is worth noting that a decrease in fluorescence can also originate from some other sources. To study the roles of these possible causes will enable us to obtain a clearer understanding of the observation. In this subsection and the next, we will, respectively, discuss two of these sources, i.e., saturation-induced hole burning and optical pumping into a natural dark state decoupled from the exciting field (here “*natural*” is used to distinguish from the dark state formed by superposition).

Due to the small reflection ($< 3\%$) of the laser by the chamber window, a weak standing wave $\sigma^+ - \sigma^+$ may be formed. This standing wave may lead to saturation holes, i.e., a Lamb hole and a crossover hole in fluorescence. For the Lamb hole, this is because the total absorption of both counterpropagating waves has a minimum at $\omega'_L = \omega_A$, where the effective laser frequency is $\omega'_L = \omega_L - \tan \alpha_m z$, with $\tan \alpha_m = \gamma b [g_e m - g_g (m-1)]$, for a $|F_g, m-1\rangle \rightarrow |F_e, m\rangle$ transition at a place z . Since the rate of energy

absorption from the laser field is equal to the atomic fluorescence, we may expect a dip to occur in the fluorescence profile. A similar reason can account for a crossover hole. The centers of these holes are situated, for the Lamb cases at,

$$\begin{aligned} z_L &\approx \cot \alpha_m \delta, & z_L &\approx \cot \alpha_m (\delta + \Delta_{23}), \\ z_L &\approx \cot \alpha_m (\delta + \Delta_{13}), \end{aligned} \quad (42)$$

corresponding to the L_3 transition, the L_2 transition ($F_g = 2 \rightarrow F_e = 2$), and the L_1 transition ($F_g = 2 \rightarrow F_e = 1$), respectively; and for crossover cases at

$$z_c \approx \cot \alpha_m \left(\delta + \frac{1}{2} \Delta_{23} \right), \quad z_c \approx \cot \alpha_m \left(\delta + \frac{1}{2} \Delta_{13} \right), \quad (43)$$

corresponding to coherent transitions $|F_g = 2, m - 1\rangle \rightarrow |F_e = 2, 3, m\rangle$ and $|F_g = 2, m - 1\rangle \rightarrow |F_e = 1, 3, m\rangle$, respectively. In Eqs. (42) and (43), Δ_{j3} is the energy difference between two hyperfine excited levels $F_e = j$ and $F_e = 3$, with $\Delta_{23} = 2\pi \times 267$ MHz and $\Delta_{13} = 2\pi \times 424$ MHz. Equations (42) and (43) indicate that (i) for different detuning, the burned holes should be located at different place along the beam; and (ii) the holes cover the zero-field point only when $\delta \approx 0$, $-\Delta_{23}/2$, $-\Delta_{13}/2$, and $-\Delta_{23}$, respectively. To see these holes more clearly, we used a retroreflection mirror outside the chamber to form a strong standing wave. It was thus observed clearly that when the laser frequency was scanned, in addition to the dark region remaining nearly still at the zero-field point, an additional dark region moved along the fluorescence beam. The coincidence of the locations of these second dark regions with the prediction was verified by simultaneously monitoring the saturation absorption spectrum on an oscilloscope. Furthermore, the second dark region was different from the central one in another aspect: When applying a polarizer in front of the CCD and rotating its transmission optical axis, the former would always be dark while the latter was alternately bright and dark. This fact may serve as further evidence to prove that our identification of the second dark region with the saturation hole, which is less affected by the radial magnetic field, is correct. Therefore, the saturation hole is not the reason for the dip at $z \approx 0$, while it may lead to some asymmetry in the profile because of its detuning-dependent location.

For the scheme of a 1D σ^+ - σ^- standing wave, a more interesting phenomenon can be observed. There may be two additional dark regions that appear symmetrically relative to the central one; when the laser frequency is scanned, they will move in counter directions. This can be easily understood because the Zeeman splitting is reversed on two sides of $z = 0$, and thus the places for resonance transitions excited by σ^+ and σ^- lights are symmetrical. This phenomenon can still be observed in MOT's, as these dark regions can move out of the intersecting region, while the central dark region becomes invisible.

D. Optical pumping to natural dark states

In Sec. III, it was shown that the velocity may not change the qualitative result from the nonadiabatic approximation.

However, the velocity will in fact cause a Doppler shift which may excite the other hyperfine transitions, i.e., $F_g = 2 \rightarrow F_e = 2, 1$. For these transitions, the natural dark states, which are not optically connected to the excited state, can be (i) $F_g = 1$, since there is no repump laser (the separation between two ground hyperfine levels is about $2\pi \times 6$ GHz); and (ii) $|F_g = 2, m = 2\rangle$ for the L_2 transition and $|F_g = 2, m = 1, 2\rangle$ for the L_1 transition. For case (i), one may expect the largest decrease of fluorescence on resonance of the $L_2(L_1)$ transition (due to the selection rule, an atom cannot decay to $F_g = 1$ for the L_3 transition), which may occur at the same locations as the Lamb holes for these transitions. This means that the location should move along with the scanning of laser frequency. On the other hand, the population loss due to a drop to the trapped level $F_g = 1$ will contribute to another part of the asymmetry of the fluorescence profile. This can be seen if we replace N in I_f by $N(1 - n_z)$, where $n_z = W(v_z)dv_z$, with velocity components $v_z \approx (\delta - \Delta_{2(1)3} - \tan \alpha_m z)/K_L$, is the population loss. For case (ii), we can see that they are actually not dark states in a strict sense, because they are destroyed by the magnetic dipole transition. The competition between the optical pumping and the magnetic moment precession determines the population trapped in these states. Taking $|F_g, m = F_g\rangle$ for example, the stationary trapped population can be estimated to be $\sim \Gamma_p / (\Gamma_p + \Gamma_B)$, where $1/\Gamma_B$ is the lifetime of the sublevel, induced by the coupling Ω_B with the adjacent one $|F_g, m = F_g - 1\rangle$, which has a width Γ_p resulting from an optical coupling to an excited state with a natural width Γ :

$$\begin{aligned} \Gamma_B &= \frac{\Gamma_p |\Omega_B|^2 / 2}{\Gamma_p^2 / 4 + \delta_B^2}, \\ \Gamma_p &= \frac{\Gamma |\Omega_0|^2 / 2}{\Gamma^2 / 4 + \delta_p^2}, \\ \delta_p &= \delta_v - \tan \alpha_m z, \end{aligned} \quad (44)$$

$$|\Omega_B| \sim \gamma_g B_\rho,$$

$$\delta_B = f_B - (\omega_{m-1}^g - \omega_m^g) = \gamma_g B_z - \Delta_{m-1},$$

where f_B is the radial magnetic field frequency which is zero, and $\Delta_{m-1} = \delta_p / \Gamma \Gamma_p$ is the light shift of the sublevel $m = F_g - 1$. Since mainly atoms with v_z satisfying the resonant L_2 transition are possibly trapped in $|F_g, m = F_g\rangle$, we may set $\delta_p = 0$ for simplicity, and obtain

$$\frac{\Gamma_p}{\Gamma_p + \Gamma_B} \sim \frac{|\Omega_0|^4 + \Gamma^2 \gamma_g^2 b^2 z^2}{|\Omega_0|^4 + \Gamma^2 \gamma_g^2 b^2 z^2 + \frac{1}{8} \Gamma^2 \gamma_g^2 b^2 \rho^2}. \quad (45)$$

Equation (45) shows that the population trapped in $|F_g, m = F_g\rangle$ will behave like the orientation M_z obtained for the $F_g \rightarrow F_e = F_g + 1$ transition in Sec. III. A difference between the two transitions is that the σ^- and π -polarized fluorescences for the $F_g \rightarrow F_e = F_g$ transition are both proportional

to the population of the sublevel $|F_g, m = F_g - 1\rangle$, because $|F_g, m = F_g\rangle$ is a dark state in terms of the optical excitation. Since the atom number of $|F_g, m = F_g - 1\rangle \sim \Gamma_B / (\Gamma_p + \Gamma_B)$, this fact infers that not only $I_x(\mathbf{e}_x)$, but also $I_x(\mathbf{e}_y)$ will have a peak at $z=0$, and leads to a peak rather than a dip in the unpolarized fluorescence. We can conclude that the contribution of the atoms who satisfy the resonant $F_g \rightarrow F_e = F_g$ transition will in effect smear the contrast of the dip.

E. Further remarks

The similar central dark regions observed in 1D $\sigma^+ - \sigma^+$ and $\sigma^+ - \sigma^-$ configurations can be interpreted in terms of the same physical picture as that for a 1D σ^+ traveling wave, except for some small adaptations in actual analysis. These adaptations can be as follows.

First, for the case of a 1D $\sigma^+ - \sigma^-$ configuration, the above model, with $J_g = 1/2$, should be replaced by a model with $J_g \geq 1$. This is because, according to the previous analysis, in order to obtain a fluorescence decrease there needs to be at least one sublevel, with a smaller Clebsch-Gordan coefficient coupling to both σ^+ and σ^- lights, for atoms from the most light-shifted sublevels (i.e., $m = \pm J_g$) to precess to. Second, one may have to include the cooling effect in these configurations [31,39–43], especially for those atoms whose interaction time with the light ($\leq 2R/v_\rho$) is comparable to the cooling and trapping characteristic time scales; i.e., the velocity relaxation time β/M and the position damping time k/β , where M is the mass of the atom, and β and k are friction and spring parameters. To take account of the cooling effect may result in two consequences: (i) the velocity v_z is no longer a conservative variable, and (ii) the atomic density N cannot remain homogeneous everywhere in space. However, so far as the one dimensional case is concerned, these effects will be very weak because the cooling time is short for most atoms.

For the case of a linearly polarized laser, as we analyzed in Sec. III, the phenomenon can be understood as a result of a combination of a classical Hanle effect and optical double resonance when near resonance. When off resonance, however, the situation will be complex, as we should further include the Λ - or M -CPT for $F_g = 2 \rightarrow F_e = 2, 1$ transitions established by σ^+ and σ^- laser components [22,23].

V. CONCLUSIONS

In conclusion, we reported an experimental observation of a dark region, about the zero-field point of a quadrupole magnetostatic field, in spatial fluorescence emitted by dilute vapor atoms, which were excited by a circularly polarized traveling wave laser tuned to a resonant $\Delta F = 1$ transition of the ^{87}Rb D_2 line. A theoretical analysis showed that this phenomenon is mainly a result of a competition between optical pumping and precession of magnetic dipole moments due to a radial magnetic field. The latter will mostly cancel the orientation caused by the former at the level crossing, where the radial dc magnetic field which couples the Zeeman sublevels is on resonance. The phenomenon can be understood, from an alternative point of view, as a result of de-

structive quantum interference between different atomic transition pathways, which is induced by a coherent interaction with two fields: one is a laser field, and the other is radial magnetic field. Our analytical expressions for the fluorescence intensity can explain the experimental result qualitatively. A quantitative comparison between theory and experiment may need a more precise calculation, including the real transition $F_g = 2 \rightarrow F_e = 3$. Moreover, since our above calculation is general, we expect that a similar phenomenon may occur for other kinds of atoms.

Our observation demonstrates that the radial magnetic field is important in the interaction of an atom with both light and a 3D magnetic field. However, its role has been neglected in current theories about cooling and trapping process in MOT's. Although the MOT has become a widely used simple source of cold atoms, the interpretation of the trapping mechanism in it is not simple, and a full understanding of the MOT has not yet been reached. Initially, the atom behavior in MOT's was estimated based on Doppler radiation force with a 1D model, which takes account of only a 1D quadrupole magnetic field, i.e., a purely longitudinal field parallel to the laser axis. It was later realized that the polarization gradient cooling of the laser, exploiting the atom's Zeeman manifold structure, is also important [31,42,43]. Stimulated by the investigation of Molmer [44] on sub-Doppler cooling in a three-dimensional laser in the absence of a magnetic field, Steane *et al.* [31] further extended the 1D model of a MOT to a model containing a 3D laser, in which the magnetic fields are still 1D (related to each dimensional laser beam). So far, the effect of a 3D magnetic field on polarization gradient cooling in MOT's has not received much attention, although numerical calculations by Raab *et al.* [45] showed that the presence of a 3D magnetic field may result in a different Doppler radiation force compared to that with only a 1D magnetic field. As we know that a radial magnetic field, combined with a proper light arrangement such as 1D $\sigma^+ - \sigma^+$ standing wave, can produce a sub-Doppler cooling [39–41], we expect that the involvement of a radial magnetic field may give some adaptation of the present theory of MOT's and remove some discrepancy between the theory and the experiments [43]. The influence of a radial magnetic field on the polarization gradient cooling in MOT's may be illustrated in an intuitive way: Taking a 1D $\sigma^+ - \sigma^-$ configuration, for example, in an atomic moving rotating frame with the quantization axis chosen along the laser polarization \mathbf{E} [46], supposing \mathbf{B}_ρ is parallel to \mathbf{E} at some point, then after a quarter-wave space \mathbf{B}_ρ will be perpendicular to \mathbf{E} , and after a half-wave space be antiparallel to \mathbf{E} , and the reverse thereafter. This induces that, due to the Zeeman shift by \mathbf{B}_ρ , the energy difference between the ground sublevels with $\Delta m = 2$, e.g., g_{+1} and g_{-1} in Ref. [46], should vary periodically along with the position and no longer be flat. Therefore, the cooling mechanism may be somewhat different. On the other hand, the work of Dalibard and Cohen-Tannoudji [46] tells us that the sub-Doppler cooling originates from an enhancement of a radiation pressure imbalance that is due to a motion-induced [more exactly, in MOT's, a $\tilde{v}_z = v_z + (\hbar \gamma B_z / K_L)$ effective-motion-induced] population difference between g_{+1} and g_{-1} . The introduc-

tion of B_ρ may lead to a cancellation of this atomic orientation. Therefore, the sub-Doppler cooling becomes less efficient for nonzero B_ρ . This result may not be meaningless, because a laser beam cannot be widthless, or at least cannot be very much thinner than the characteristic length ρ_c . A more strict study of this topic is needed, but that is beyond the scope of this paper.

Another consequence of the research presented here is relevant to the choice of the repump laser used in a MOT. For ^{87}Rb , for instance, where the MOT beam is tuned to the red of the $F_g=2 \rightarrow F_e=3$ transition, one usually chooses a laser tuned to the resonance of a $F \rightarrow F+1$ transition (i.e., $F_g=1 \rightarrow F_e=2$) instead of a $F \rightarrow F$ transition as a repump laser. This is partly because, for circularly polarized light, the latter may optically pump atoms into an inaccessible state, and hence decrease the repumping efficiency. However, the study of this paper shows that if using a circularly polarized laser, even for a $F \rightarrow F+1$ transition, there are still some atoms which, near the trap center, will be confined in the lower hyperfine level of ground state, due to the presence of a radial magnetic field, and cannot be pumped to a higher hyperfine level. Therefore, in order to increase repumping efficiency (for a bright MOT), we should exploit a repump beam of not-too-weak power to reduce the confinement effect (of course, the very low intensity itself will also provide a poor repumping rate). On the other hand, our study also shows that using a standing wave or a 3D repump laser, which can partially reduce the darkness in the central region, may be more favorable for a MOT than a 1D circularly polarized traveling wave.

A direct application of the effect we observed is in the alignment of three pairs of $\sigma^+ - \sigma^-$ laser beams in a MOT to make the center of their intersecting region overlap the magnetic-field zero. We have found that if the two points do not coincide very well, when one transfers a MOT to an optical molasses by quickly shutting down the magnetic field, atoms may feel a push directed from the MOT center to the molasses center. The push is associated with a dipole force pointing to the place of maximum light intensity, i.e., the molasses center, as the molasses beams are red-detuned Gaussian ones [47]. Since statistically low-velocity atoms are closer to the MOT center than those of large velocity, they will be more sensitive to the displacement of the two centers. Therefore, the push is actually a heating. The amount of the heating may be roughly estimated as $\Delta T = (M \omega_{op}^2 / k_B) r^2$, assuming the optical potential can be approximated as a harmonic form, where k_B is the Boltzmann constant, ω_{op} is the oscillation frequency of the optical potential, and r is the separation between two centers. The heating introduced in the transfer process may greatly affect the temperature and atom number of the molasses. The displacement of the two points may be reduced by aligning the beams while measuring and minimizing the molasses temperature. Now, by exploiting the phenomenon observed, we can make this task easier to fulfill, because we can directly see, on a CCD video screen, where the zero-field point is. An advantage of this method is that if any stray magnetic field is added to the quadrupole field from the trapping coils (it merely shifts the zero of the field), we can quickly find out

the location of the new trap center. In experiment, we can first locate the zero-field point by a 1D $\sigma^+ - \sigma^-$ beam, then align the other two orthogonal pairs of beams to make each of their central axes lie on the dark region. In this way, we have achieved satisfying molasses cooling.

The phenomenon can also be applied to measure the magnetic field in the vacuum chamber [30]. With a 1D $\sigma^+ - \sigma^+$ standing-wave diode laser, by scanning the laser frequency near the $1 \rightarrow 2$ transition, and at the same time recording the corresponding distance between the center of the central dark region and that of the Lamb hole (with a width of the same order of magnitude as the central region), we can determine the magnetic-field gradient near the field origin in terms of a relation between the laser detuning and the dark region separation, $b \approx [1/(2g_e - g_g)](\delta/z_L)$, deduced from Eq. (42), where we have let $m=2$ due to the optical pumping effect. We have found a good agreement between the experimentally measured values and the theoretically calculated values from a formula given in Ref. [35], by including a nonunit magnetic susceptibility, because our coils were mounted on chamber windows, not within the vacuum, which was the case considered in Ref. [35]. This result, combined with the dark region around the field zero, opens up the possibility for measuring an unknown magnetic field by using a calibrated quadrupole field, especially in places where traditional means, such as the Gauss meter, are not convenient to apply. This may offer another type of quantum-interference-based magnetometer in addition to the recently introduced one which exploits the CPT effect [22].

ACKNOWLEDGMENTS

The authors would like to thank H. Metcalf, E. Arimondo, F. Renzoni, F. L. Li, and T. Pfau for helpful discussions. This work was supported by the Ministry of Science and Technology of China under Grant No. 95-Yu-34, and the National Natural Science Foundation of China No. 19834046. Q.L. was supported by the Chinese Postdoctoral Science Foundation.

APPENDIX

From Eq. (37), we obtain the zeroth, first, second, etc. orders of M_z , with

$$M_{z0} = 1,$$

$$M_{z1} = 0,$$

$$M_{z2} = a_{20}, \quad (\text{A1})$$

$$M_{z3} = a_{31}z + a_{30},$$

$$M_{z4} = a_{42}z^2 + a_{41}z + a_{40},$$

...

where

$$a_{20} = \frac{27}{2} \gamma^2 \left[-\frac{\rho^2}{9f^2 + \Gamma_p^2} + \frac{6(9f^2 + 2\Gamma_p^2)v_\rho \rho}{\Gamma_p(9f^2 + \Gamma_p^2)^2} - \frac{27(9f^2 + 2\Gamma_p^2)v_\rho^2}{\Gamma_p^2(9f^2 + \Gamma_p^2)^2} \right],$$

$$a_{31} = -\frac{486\gamma^3 f[\Gamma_p^2(\rho\Gamma_p - 9v_\rho)^2 + 9f^2(27v_\rho^2 - 6\rho v_\rho \Gamma_p + \rho^2 \Gamma_p^2)]}{\Gamma_p^2(9f^2 + \Gamma_p^2)^2}, \quad \dots,$$

and $f = \dot{\phi} - 2\Delta$. Here we are only concerned about the coefficients of z^n , while for larger n the expressions of $a_{n,m}$ will be rather lengthy. We may simplify them by assuming $f \approx 0$. Since $\dot{\phi} = (v_y \cos \phi - v_x \sin \phi)/\rho$, combined with the condition for nonadiabatic evolution $\rho \sim v/\Gamma_p$, we have $\dot{\phi} \sim \Gamma_p$. Therefore, $f \approx 0$ is equivalent to assuming $|\Gamma/2 - \delta_v| \ll 1/s_0$. Under this assumption, we have

$$a_{31} = 0,$$

$$a_{42} = \frac{486\gamma^4(\rho\Gamma_p - 9v_\rho)^2}{\Gamma_p^6}, \quad (\text{A2})$$

$$a_{41} = -\frac{1458\gamma^4 v_z}{\Gamma_p^7} [81(10 + v_z)v_\rho^2 - 18(7 + v_z)\Gamma_p \rho v_\rho + 2(2 + v_z)\Gamma_p^2 \rho^2].$$

It can be seen that if taking $v_\rho, v_z, \dot{\phi}$ to be zero, the solution $M_z = M_{z0} + bM_{z1} + b^2M_{z2} + b^3M_{z3} + b^4M_{z4} + \dots$ will return to the corresponding expansion of Eq. (30) in b .

[1] See, for example, S. Haroche and D. Kleppner, *Phys. Today* **44** (1), 24 (1989); B. L. Lü, Y. Z. Wang, Y. Q. Li, and Y. S. Liu, *Opt. Commun.* **108**, 13 (1994); Y. Z. Wang, B. L. Lü, Y. Q. Li, and Y. S. Liu, *Opt. Lett.* **20**, 1 (1995); C. Hood, M. Chapman, T. Lynn, and H. Kimble, *Phys. Rev. Lett.* **80**, 4157 (1998).

[2] See, for example, C. W. Gardiner, *Phys. Rev. Lett.* **56**, 1917 (1986); H. J. Carmichael, A. S. Lane, and D. F. Walls, *ibid.* **58**, 2539 (1987); H. M. Wiseman, *ibid.* **81**, 3840 (1998); P. Rice and C. Baird, *Phys. Rev. A* **53**, 3633 (1996).

[3] H. J. Eberly, *Phys. Rev. Lett.* **37**, 1387 (1976); G. S. Agarwal, *Phys. Rev. A* **18**, 1490 (1978); P. Zoller, G. Alber, and R. Salvador, *ibid.* **24**, 398 (1981); K. Wodkiewicz, B. W. Shore, and J. H. Eberly, *ibid.* **30**, 2390 (1984); R. Vyas and S. Singh, *ibid.* **45**, 8095 (1992); P. Zhou and S. Swain, *ibid.* **58**, 4705 (1998).

[4] W. Tan and M. Gu, *Phys. Rev. A* **34**, 4070 (1986); V. Buzek, *ibid.* **39**, 2232 (1989).

[5] T. Walker, D. Sesko, and C. Wieman, *Phys. Rev. Lett.* **64**, 408 (1990); D. Sesko, T. Walker, and C. Wieman, *J. Opt. Soc. Am. B* **8**, 946 (1991).

[6] D. A. Cardimona, M. G. Raymer, and C. R. Stroud, Jr., *J. Phys. B* **15**, 55 (1982).

[7] S. E. Harris, *Phys. Rev. Lett.* **62**, 1033 (1989).

[8] A. Imamoğlu and S. E. Harris, *Opt. Lett.* **14**, 1344 (1989).

[9] A. Imamoğlu, *Phys. Rev. A* **40**, 2835 (1989).

[10] P. Zhou and S. Swain, *Phys. Rev. Lett.* **77**, 3995 (1996); *Phys. Rev. A* **56**, 3011 (1997).

[11] P. R. Berman, *Phys. Rev. A* **58**, 4886 (1998).

[12] H. R. Gray, R. M. Whitley, and C. R. Stroud, Jr., *Opt. Lett.* **3**, 218 (1978).

[13] P. L. Knight, *Opt. Commun.* **32**, 261 (1980).

[14] E. E. Fill, M. O. Scully, and S. Y. Zhu, *Opt. Commun.* **77**, 36 (1990).

[15] L. M. Narducci, M. O. Scully, G. L. Oppo, P. Ru, and J. R. Tredicce, *Phys. Rev. A* **42**, 1630 (1990).

[16] L. M. Narducci, H. M. Doss, P. Ru, M. O. Scully, S. Y. Zhu, and C. Keitel, *Opt. Commun.* **81**, 379 (1991).

[17] A. Imamoğlu, J. E. Field, and S. E. Harris, *Phys. Rev. Lett.* **66**, 1154 (1991).

[18] K. J. Boller, A. Imamoğlu, and S. E. Harris, *Phys. Rev. Lett.* **66**, 2593 (1991).

[19] S. Boublil, A. D. Wilson-Gordon, and H. Friedmann, *J. Mod. Opt.* **38**, 1739 (1991).

[20] Y. Z. Wang, G. Xu, C. Ye, J. M. Zhao, S. Y. Zhou, and Y. S. Liu, *Phys. Rev. A* **53**, 1160 (1996).

[21] H. Y. Ling, Y. Q. Li, and M. Xiao, *Phys. Rev. A* **53**, 1014 (1996).

[22] F. Renzoni, W. Maichen, L. Windholz, and E. Arimondo, *Phys. Rev. A* **55**, 3710 (1997).

[23] F. Renzoni and E. Arimondo, *Phys. Rev. A* **58**, 4717 (1998).

[24] A. Aspect, E. Arimondo, R. Kaiser, N. Vansteenkiste, and C. Cohen-Tannoudji, *J. Opt. Soc. Am. B* **6**, 2112 (1989).

[25] E. Arimondo, in *Progress in Optics*, edited by E. Wolf (Elsevier, Amsterdam, 1996), Vol. 35, p. 257; L. V. Hau, S. E.

- Harris, Z. Dutton, and C. H. Behrooz, *Nature (London)* **397**, 594 (1999).
- [26] W. Hanle, *Z. Phys.* **30**, 93 (1924); For a review, see, for example, A. Corney, *Atomic and Laser Spectroscopy* (Oxford University Press, Oxford, 1977).
- [27] See, for example, W. Demtröder, *Laser Spectroscopy* (Springer-Verlag, New York, 1981).
- [28] Q. Long, S. Y. Zhou, S. Y. Zhou, and Y. Z. Wang, *Laser Spectroscopy XIV; Frontiers of Laser Physics and Quantum Optics, Proceedings of the International Conference*, edited by Z. Z. Xu, S.W. Xie, S. Y. Zhu, and M. O. Scully (Springer-Verlag, Berlin, 2000), p. 533; *CLEO/Pacific Rim'99* (IEEE 99TH8464), paper FF4.
- [29] L. Deng and E. W. Hagley (private communication).
- [30] S. Y. Zhou, Q. Long, S. Y. Zhou, and Y. Z. Wang (unpublished).
- [31] A. M. Steane, M. Chowdhury, and C. J. Foot, *J. Opt. Soc. Am. B* **9**, 2142 (1992).
- [32] The intensity imbalance was less than about 0.05 in our experiment, which corresponded to a maximum displacement of the trap center from the field zero of ~ 0.03 cm, for a magnetic gradient 18 G/cm. A discussion of the imbalance dependence of the trap center location can be found to Ref. [31].
- [33] The error bar of contrast is obtained by $\Delta C = 2\Delta I / (I_{\max} + I_{\min})$, where ΔI is the fluctuation of fluorescence intensity mainly due to the noises in laser and CCD. ΔI can be approximately determined by measuring the standard deviation of the fluorescence when the quadrupole magnetic field is not turned on.
- [34] These facts tell us that if a laser is elliptically polarized, the direction of the major axis of the ellipse will affect the observation result. As a pure circular polarization state is hard to realize, when doing the above experiment for circularly polarized laser we always arranged the major axis of the ellipse along the y direction in order to exclude the influence of this asymmetry on the dip.
- [35] T. Bergman, G. Erez, and H. J. Metcalf, *Phys. Rev. A* **35**, 1535 (1987).
- [36] Another way to obtain the effective laser frequency $\tilde{\omega}_L$ is the following. As the electric dipole is excited by the σ^+ laser, the electron moves along a circle with a circular frequency ω_L and a radius $|\mathbf{D}|/e$. It will experience an additional centrifugal force (Lorentz force) $f_\rho = -|\mathbf{D}|\omega_L B_z$ in the presence of B_z . We then have the modified force $\tilde{f}_\rho = (m/e)|\mathbf{D}|\tilde{\omega}_L^2 = (m/e)|\mathbf{D}|\omega_L^2 + f_\rho$; therefore $\tilde{\omega}_L^2 = \omega_L(\omega_L - 2\gamma B_z)$. For $\omega_L \gg \omega_z$, we have $\tilde{\omega}_L^2 \approx (\omega_L - \omega_z)^2$.
- [37] M. Sargent III, M. O. Scully, and W. E. Lamb, Jr., *Laser Physics* (Addison-Wesley, Reading, MA, 1974).
- [38] A recent experiment shows that this is very likely the right reason. In this experiment, we added a repump laser tuned to resonance of $1 \rightarrow 2$ transition which, combined with the $2 \rightarrow 3$ transition, could form a nearly closed system. It was found that the contrast of the dip was affected little when the power of the pump laser was weak, while, when its intensity was high, the darkness degraded evidently compared to that without a repump laser.
- [39] D. S. Weiss, E. Riis, Y. Shevy, P. J. Ungar, and S. Chu, *J. Opt. Soc. Am. B* **6**, 2072 (1989).
- [40] B. Sheehy, S. Q. Shang, P. Van Straten, S. Hatamian, and H. Metcalf, *Phys. Rev. Lett.* **64**, 858 (1990).
- [41] S. Q. Shang, B. Sheehy, P. Van Straten, and H. Metcalf, *Phys. Rev. Lett.* **65**, 317 (1990).
- [42] A. M. Steane and C. J. Foot, *Europhys. Lett.* **14**, 231 (1991).
- [43] M. Drewsen, P. Laurent, A. Nadir, G. Santarelli, A. Clairon, Y. Castin, D. Grison, and C. Salomon, *Appl. Phys. B: Lasers Opt.* **59**, 283 (1994).
- [44] K. Molmer, *Phys. Rev. A* **44**, 5820 (1991).
- [45] E. L. Raab, M. Prentiss, A. Cable, S. Chu, and D. Pritchard, *Phys. Rev. Lett.* **59**, 2631 (1987).
- [46] J. Dalibard and C. Cohen-Tannoudji, *J. Opt. Soc. Am. B* **6**, 2023 (1989).
- [47] J. P. Gordon and A. Ashkin, *Phys. Rev. A* **21**, 1606 (1980).